Proceedings of the
Annual Stability Conference
Structural Stability Research Council
San Antonio, Texas, March 21-24, 2017

Stability of Slender Section H.S.S. Columns

Liya Li[1], Lucile Gérard[2], Marielle Hayeck[3], Nicolas Boissonnade[4]

Abstract

This research is focused on the behavior and response of hollow section columns having slender cross-sections. Columns typically concerned with sections affected by local buckling are made of quite thin-walled tubular shapes and/or high strength material. Unlike for classical columns, the detrimental influence of local instability and its coupling with flexural buckling is so strong that it cannot be neglected in design, and deserves adequate treatment.

As a major difficulty to a safe but accurate treatment of such columns, the way the local/global coupled instabilities depends on the member's length and on the interaction with yielding is essential. This, however, remains a complex and challenging situation within Structural Engineering.

The present paper details numerical investigations that aimed at providing a deeper understanding of the combined phenomena involved. Using hundreds of suitable shell F.E. results as a database of reference results, the mechanical response of such members is carefully characterized and improved design recommendations are proposed.

1. Introduction

Recent construction practice has seen a rise in the use of structural hollow sections, due to their appealing aesthetics and advantages in terms of strength and stiffness. In order to meet the increasing demands for sustainable and economic construction, the European steel industry, and particularly the producers of structural hollow sections, are aiming for a reduction of weight and cost saving through the use of more thin-walled sections and/or higher-strength steel grades (with yield strength $f_y \geq 460\ MPa$). These innovations increase the economy and sustainability of construction projects through the reduction of weld volumes, erection times and foundation costs. Especially, the introduction of higher-strength steel grades into standard construction practice can be seen as a relevant industrial goal for the steel industry, offering chances for new product development, research and innovation, and thus market advantages.

However, the introduction of more slender hollow sections leads to a number of scientific and engineering challenges: higher material strength with different constitutive laws (shorter or inexistent plastic plateau, diminished ultimate strain) combined with thinner plates leads to an

[1] Graduate Student, Chang'an University, Xi'an, China, <liya_chd@outlook.com>
[2] Graduate Student, Laval University, <lucile.gerard.1@ulaval.ca>
[3] PhD, <marielle_hayeck@hotmail.com>
[4] Professor, Laval University, <nicolas.boissonnade@gci.ulaval.ca>

increased significance of instability phenomena, especially of local buckling phenomena and their interaction with the global instability mode of flexural buckling. At the level of cross-sectional resistances, an increase in yield strength leads to an increase in normalized slenderness. This means that more sections fall into the slender range and are thus more sensitive to local buckling.

Preliminary studies have shown that the application of current design codes (e.g. the Eurocodes) is either ineffective, uneconomical or – in some cases – altogether impossible for combined instability phenomena in slender, high-strength hollow sections. Combined, these sortcomings represent an obstacle to the further development and use of more slender hollow section members. In order to overcome these difficulties, innovative design methods must be introduced.

The main goal of this paper consists in improving part of this situation with a focus on high strength steel tubular members, where both local and global instabilities play a significant role, by means of the "Overall Interaction Concept" (O.I.C.). This concept, through the generalization of the relative slenderness notion, sets a general, simple, effective and sound framework to the design of all structural elements. Taking due account of resistance and stability phenomena, the O.I.C. further incorporates the effects of imperfections to accurately predict the real behavior of members, as illustrated in Figure 1.

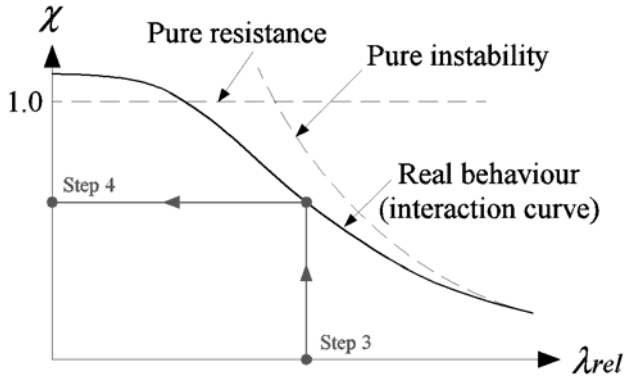

Step 1: R_{RESIST} — *Load ratio to reach the 'resistance' limit*

Step 2: R_{STAB} — *Load ratio to reach the 'instability' limit*

Step 3: $\lambda_{rel} = \sqrt{\frac{R_{RESIST}}{R_{STAB}}}$

Step 4: $\chi = f(\lambda_{rel})$

Step 5: $R_{REAL} = \chi \cdot R_{RESIST}$

Figure 1: Resistance – stability interaction for flexural buckling

The proposed O.I.C. approach relies on the generalization of the relative slenderness factor defined as $\lambda = \sqrt{R_{RESIST} / R_{STAB}}$, where R_{RESIST} represents the factor by which the initial loading has to be multiplied to reach the pure resistance limit and R_{STAB} is the equivalent factor used to reach the buckling load (instability) of the ideal member. Doing so makes it capable of dealing with complex loading situations, as well as with various problems (e.g. member or cross-section resistance-instability interaction, non-linear material behavior…). The relative slenderness "λ"leads to the determination of a "χ" value called "reduction factor" that represents the penalty due to instability effects on the pure resistant behavior, leading to the final "real" resistance that accounts for both instability effects, resistance aspects and the influence of imperfections.

The following section 2 first describes modelling assumptions used within the present numerical studies: meshing, loading and support conditions, material and geometrical imperfections, adopted material law…Then, it describes extensive numerical simulations performed that served as a basis to investigate the structural response of high strength steel tubular structures tested under an axial compressive load.

Section 3 and 4 provide F.E. results related to behavior and design of compact to slender high strength steel beam-column members. The results are presented in the O.I.C. format, and continuous interaction curves are presented, for hot-rolled and cold-formed steel hollow beam-column members as a function of the member's slenderness. The particular case of very slender members (exaggeratedly slender cross-sections) demonstrated some kind of special phenomena – poorly addressed in literature – not so obvious to treat in traditional ways. A special care was paid to the design of these members that represent a special group of elements, through two different procedures: curve-fitting α - values and local/global interaction factors.

Eventually, actual and future research directions are finally addressed in section 5.

2. Finite element model assumptions

Numerical computations have been led with the use of non-linear F.E. software FINELg (Greish and ULg, FINELg 1999), continuously developed at the University of Liège and Greisch Engineering Office since 1970. This software offers almost all types of F.E. analyses, and present investigations have made use of so-called G.M.N.I.A. analyses (Geometrically and Materially Non-linear with Imperfections) to determine the ultimate resistance of sections or members (Boissonnade N. and Somja H. 2012). Prior to the present investigations, F.E. models have been developed in a manner to best fit the properties of a real member and to simulate test conditions on high strength steel members as closely as possible – see U.A.S. Western Switzerland – Fribourg tests (Hayeck M. 2016) and another set from the literature (Semi-Comp 2007). It was found that the F.E. models were capable of accurately replicating the response and resistance of the experiments.

In order to quantify the interaction between local and global buckling, members have been modelled in shell elements where potential interactions between local and global instabilities are considered. Shell modelling has also been used to determine the ultimate resistance and witness local buckling of a cross-section; in such cases, the length of the specimens was chosen equal to three times the largest cross-sectional dimension in order to avoid a too severe influence of global buckling.

Sections (i.e. very short members) were modelled by means of quadrangular 4-nodes plate-shell finite elements with typical features (corotational total lagrangian formulation, Kirchhoff's theory for bending) and *members* have been modelled with a regular mesh all over the length, with corners modelled with two shell elements per corner (see Figure 2).

The support conditions and the introduction of applied loads received particular attention, and use of so-called kinematic linear constraints has been made to ensure a "plane-sections-remain-plane" behavior of the end sections. Following ideal simply-supported "fork" support conditions, end cross-sections can only exhibit a maximum of three degrees of freedom: axial global displacement, rotation about the strong axis and rotation about the weak axis. Only three different nodes are then necessary to describe the displacement of any point in the cross-section once the linear relationships for axial displacements are established, as a function of the displacement of the three "longitudinal-free" nodes. In other words, a maximum of three nodes may experience a "free" longitudinal displacement, all other nodes' x-displacements linearly depending on the longitudinal displacements of the "x-free" nodes to respect a global cross-sectional displaced configuration. The three nodes were chosen at the plate edges (near different corners) of the cross-section, and all the nodes in between were constrained to the three main nodes through linear relationships. Additional fictitious nodes have been defined at the centroids

of the end-cross-sections for the definition of “beam-like” support conditions, and transverse supports preventing from local buckling have also been implemented in each plate. External loading was applied through four concentrated forces at the member’s ends (i.e. strong, weak axis bending moments and axial forces) and has been implemented at the flanges’ plates as shown in Figure 2.

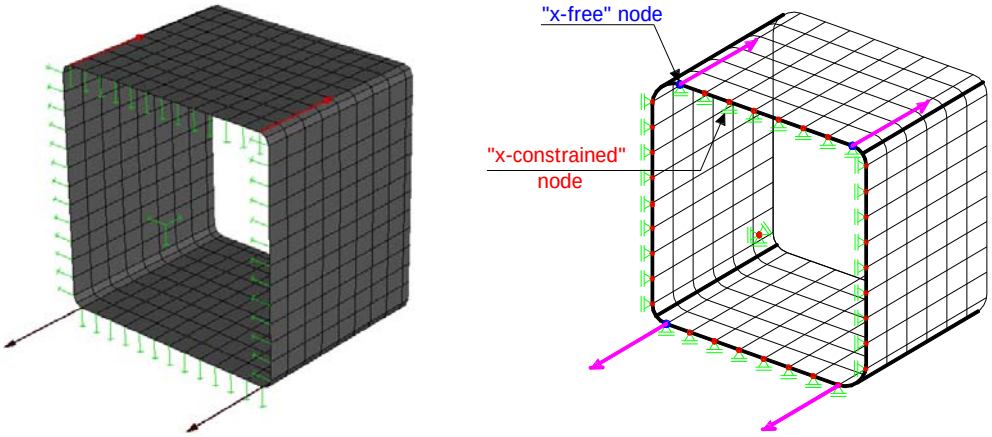

Figure 2: Loading and support conditions

An elastic-perfectly plastic material law with strain-hardening was implemented for *hot-rolled* profiles, following ECCS (ECCS 1987) and prEN 1993-1-12 (EN 1993-1-12 2007) recommendations, with different characteristics, namely regarding the plastic plateau length and available ductility.

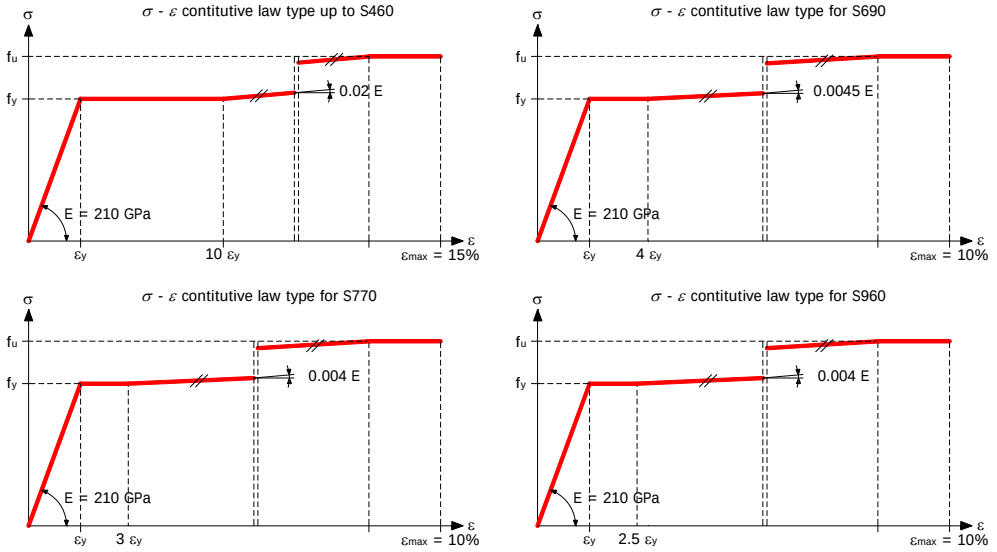

Figure 3: Elastic-perfectly plastic with strain hardening adopted material law for *hot-rolled* sections

Regarding the *cold-formed* tubular profiles, two material laws have been defined: one for the base material in the flat faces and one for the corner regions. A simple Ramberg-Osgood material law was used for the flat regions – the equations are described by Rasmussen (Rasmussen K.J.R. 2003) – and a multi-linear law was adopted for the corners region. A simple Ramberg-Osgood law was shown to be inappropriate to represent the corners region since the fibers located in these areas are characterized by a small ductility and a maximum strain of 2.5 %. Therefore,

once the section reached that level of strain, the corners would find themselves ineffective leading to the failure of the entire section and no more strains could be achieved beyond this value of 2.5% strain. However, owing to numerical needs in ductility, the specific pattern of Figure 4 was adopted, with negative stiffness allowing a reduced participation of the corners to the resistance beyond 2.5% strain.

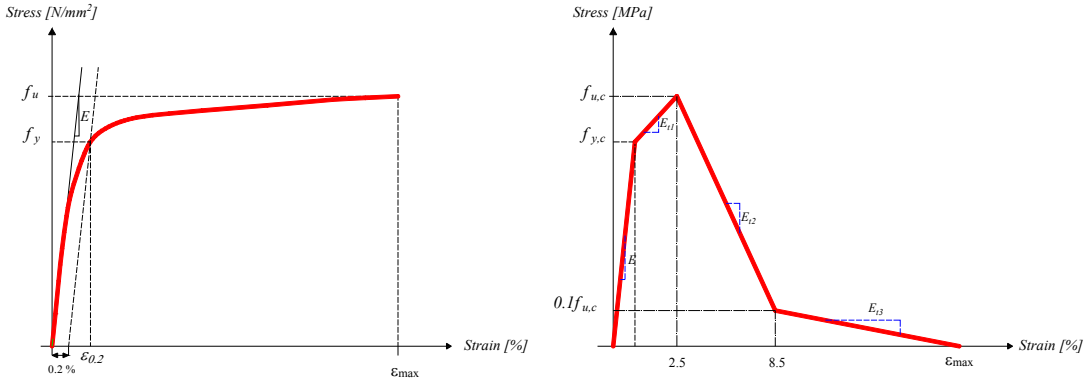

f_y < 460 *MPa*: R.-O. *coefficient: n*=22; ε_{max}=15%

f_y > 460 *MPa*: R.-O. *coefficient: n*=40; ε_{max}=10%

Figure 4: Adopted material laws for *cold-formed* sections – a) flat faces – b) corner regions

Particular attention was also paid to the modelling of residual stresses. For hot-rolled profiles, auto equilibrated membrane residual stresses patterns were generated with constant values equal to 0.5 f_y at corners and the corresponding values needed to reach equilibrium in flanges and webs (again, constant "block" distributions). The residual stresses are therefore defined so that the various stresses distributions are in auto-equilibrium in a plate-per-plate basis, as illustrated in Figure 5.

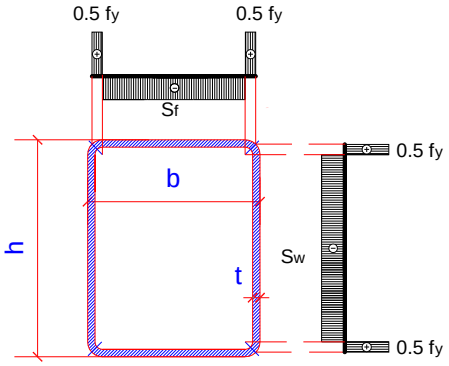

Where:

$$S_w = \frac{-0.5 f_y 4r \sin(\pi/8)}{(h-2r-t)}$$

$$S_f = \frac{-0.5 f_y 4r \sin(\pi/8)}{(b-2r-t)}$$

Figure 5: Residual stresses distribution (ensuring auto-equilibrium) for tubular hot-rolled profiles

Concerning cold-formed profiles, flexural residual stresses with a maximum amplitude of 300 N/mm^2 were introduced in the numerical model, as suggested by Key (Key P.W. 1988). As for the corner regions in which the longitudinal stresses are less important than the flat regions, a value of 235 N/mm^2 was adopted.

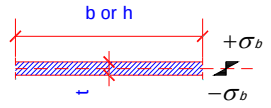

σ_b=300 *MPa*: flat region

σ_b =235 *MPa*: corner region

Figure 6: Residual stresses distribution (ensuring auto-equilibrium) for tubular cold-formed profiles

Both global and local initial geometrical defaults were taken into account in the F.E. models. *Local* imperfections shapes were introduced through an appropriate modification of node coordinates of the considered plate (i.e. web or flange) with a combination of sine waves in both directions in square half-wave patterns. Suitable inward-outward directions have been adopted to keep certain continuity in the overall pattern (see Figure 7). The adopted sine periods were equal to the average period of both constitutive plates of the section, with reasonable and realistic amplitudes of imperfections chosen as a per plate amplitude a / 200 with 'a' equal to ($b - t - 2r$) or ($h - t - 2r$) as suggested by Nseir (Nseir J. 2016).

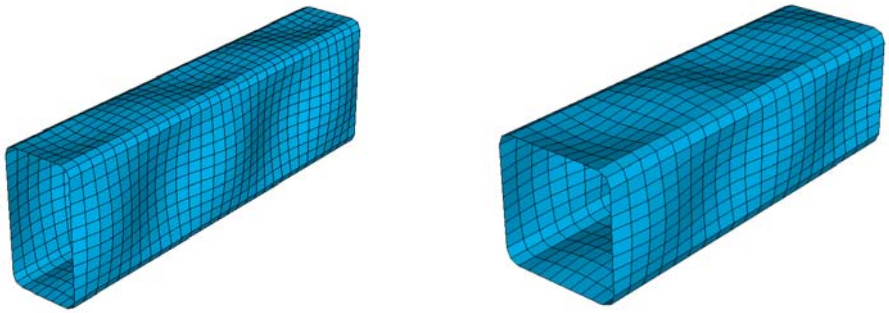

Figure 7: Local geometrical imperfections adopted for both square and rectangular hollow sections (magnified)

The initial *global* geometrical imperfections have been basically introduced through adequate modifications of node coordinates following sine shapes in both major and minor-axes with the realistic average value of global imperfection amplitude equal to L / 1000 in each principal plane, as illustrated in Figure 8.

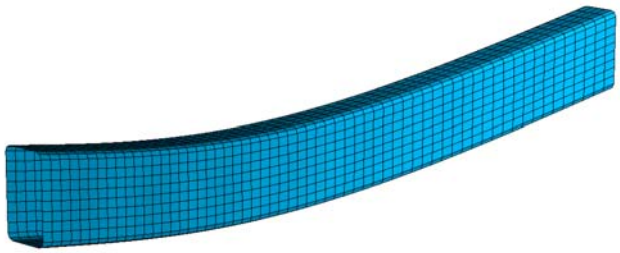

Figure 8: Magnified initial global geometric imperfections

In order to investigate how different key parameters may affect the structural response of a beam-column hollow section member, series of numerical computations on hot-rolled and cold-formed tubes have been led, covering the following parameters:

- 13 different element lengths varying from 1500 *mm* to 15000 *mm* in order to represent the whole practical range of member slenderness;
- 5 different steel grades: f_y = 235 N/mm^2, f_y = 355 N/mm^2; f_y = 690 N/mm^2; f_y = 770 N/mm^2 and f_y = 960 N/mm^2;

- 8 cross-section shapes: rectangular and square with corresponding cross-sectional classes well-distributed along class 1 and class 4 – from plastic to slender cross-section geometries – according to EN 1993-1-1 (EN 1993-1-1 2005).

Secondly, an additional set of invented sections was analyzed, in an attempt to examine the interaction between local and global instabilities under more severe circumstances (i.e. when the interaction between local and global instabilities becomes very pronounced)[5]. The proposed sections have been derived with respect to the h / b and h / t ratios, where h / b was chosen equal to 2.5 and the h / t values spanned from 15 to 115 with a step of 2.

3. Behavior and design of compact to slender high strength steel columns

In the proposed approach, cross-sectional and member resistances are based on extended Ayrton-Perry approaches (Ayrton W.E. and Perry J. 1886), providing reduction factors χ that account for potential local and global (member) instabilities. Based on the Ayrton-Perry format of Equation (1), factors α and λ_0 were fitted from numerical results.

$$\chi_{CS+MB} = \frac{1}{\phi_{CS+MB} + \sqrt{\phi_{CS+MB}^{\ 2} - \lambda_{CS+MB}^{\ 2}}} \tag{1}$$

$$\text{where } \phi_{CS+MB} = 0.5\left(1 + \alpha\left(\lambda_{CS+MB} - \lambda_0\right) + \lambda_{CS+MB}^{\ 2}\right) \tag{2}$$

All reference F.E. results were analyzed and sorted to identify the key parameters to be kept for the derivation of design curves. The following factors were determined through a best-fit procedure for hot-rolled and cold-formed sections:

- The end of plateau λ_0 value;
- The generalised imperfection factor α .

Figure 9 illustrates the application of the O.I.C. for hot-rolled square and rectangular sections under pure compression, for different steel grades. It shall be mentioned here that the O.I.C. approach for members in compression is very similar in nature to most established design provisions found in major design codes. Results for very slender sections ($\chi_{CS} < 0.6$), of high yield stresses are excluded from Figure 9, and are treated separately in section 4.

In Figure 9, the horizontal axis represents the generalized slenderness λ_{CS+MB} defined in Equation (3) while the vertical axis reports the member reduction factor χ_{CS+MB} defined in Equation (4):

$$\lambda_{CS+MB} = \sqrt{\frac{\chi_{CS}.R_{RESIST}}{R_{STAB,MB}}} \tag{3}$$

$$\chi_{CS+MB} = \frac{R_{REAL}}{\chi_{CS}.R_{RESIST}} \tag{4}$$

[5] Invented sections having highly slender components are used in order to better visualize more distributed results along higher slenderness, since European sections cover only a limited range of cross-section slenderness.

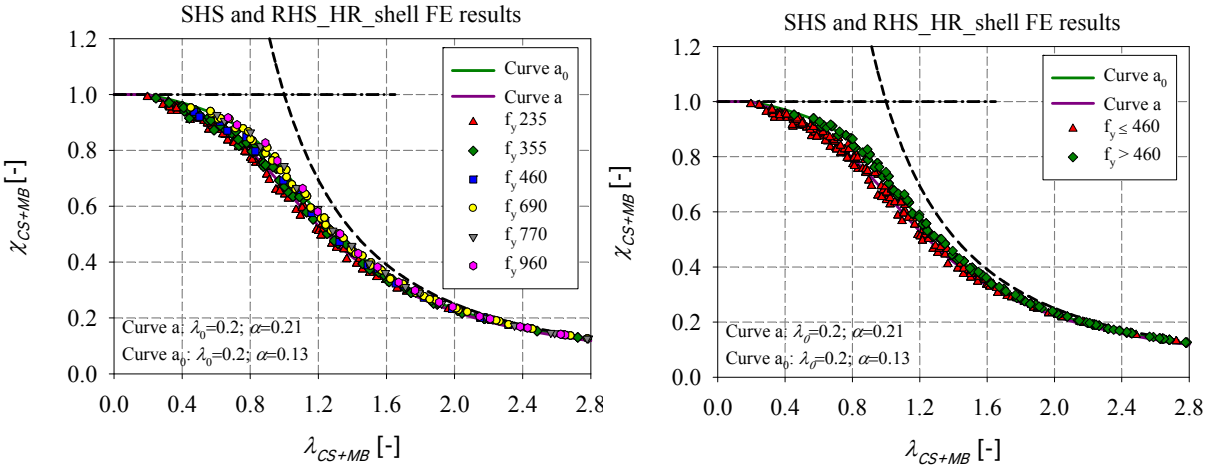

Figure 9: Shell numerical member results for *hot-rolled* SHS and RHS of different steel grades under compression

In Equation (3) and Equation (4), χ_{CS} represents the cross-section reduction factor (i.e. the penalty owing to local instability on the section's plastic capacity). In all subsequent results, χ_{CS} values have been evaluated numerically through preliminary suitable shell non-linear F.E. simulations so as to provide a fair estimation of the influence of local buckling on the members' overall responses[6].

The final resistance factor R_{REAL} was computed using shell elements so that local and global instabilities interact; R_{REAL} is therefore affected by resistance and instability as well as by initial imperfections (i.e. residual stresses, geometrical imperfections), by the material law, load case considered, section geometries, boundary conditions… R_{RESIST} represents the load ratio to reach the resistance limit and was computed using a dedicated Matlab tool developed to compute the exact capacity of the section (Epiney V. 2015); $R_{STAB,MB}$ represents the load ratio to reach the instability limit and was computed using Abaqus software with beam modelling for members (i.e. influence of cross-section instabilities is excluded).

For sake of simplicity, a single interaction curve was derived for $f_y = 235\ N/mm^2$, $f_y = 355\ N/mm^2$ and $f_y = 460\ N/mm^2$, since a small dispersion in the results was noticed – see Figure 9b. An imperfection factor α and an end-of-plateau limit λ_0 corresponding to buckling *curve a* as defined in Eurocode 3 were proposed, based on the numerical results: λ_0 was set to 0.2 and α was set to 0.21. One may notice that some numerical results lie slightly below the proposed *curve a*, indicating (limited) unsafe predictions from the proposal. This is deemed acceptable remembering the quite conservative general imperfections introduced in the numerical models.

A higher resistance is observed for $f_y = 690\ N/mm^2$, $f_y = 770\ N/mm^2$ and $f_y = 960\ N/mm^2$ and a higher curve is proposed. The imperfection factor α and the end of plateau factor λ_0 corresponding to buckling *curve a0* as defined by Eurocode 3 were proposed based on the numerical results: λ_0 was set to 0.2 and α was set to 0.13.

[6] Analytical expressions were also developed to get χ_{CS} and can be found in (Nseir J. 2015).

Numerical simulations were also performed on cold-formed rectangular and square sections tested under pure compression (see Figure 10). According to Eurocode 3, buckling *curve c* is adopted for cold-formed sections for the following nominal yield stresses: $f_y = 235\ N/mm^2$, $f_y = 275\ N/mm^2$, $f_y = 355\ N/mm^2$, $f_y = 420\ N/mm^2$ and $f_y = 460\ N/mm^2$. However, it is clearly seen from the numerical results that an increased yield stress leads to higher resistance curves. Therefore, the local-global instability phenomena is treated in structural design codes in a manner that is potentially too conservative for the high-strength hollow sections members.

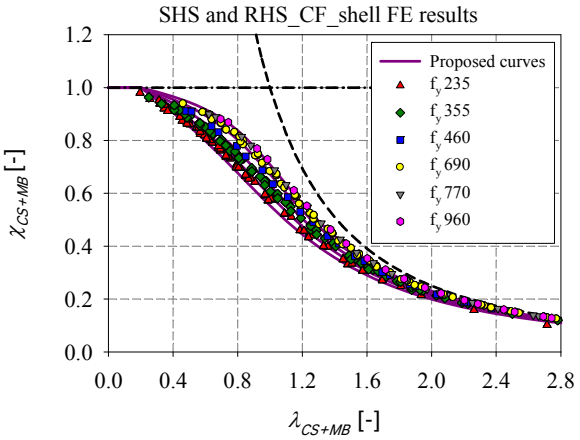

Figure 10: Numerical member results of *cold-formed* SHS and RHS of different steel grades under compression

Accordingly, multiple "design" χ_{CS+MB} interaction curves were derived for each cold-formed column depending on the corresponding steel grade and finally relationships were established between the imperfection factor α and the corresponding yield stress f_y (see Figure 11).

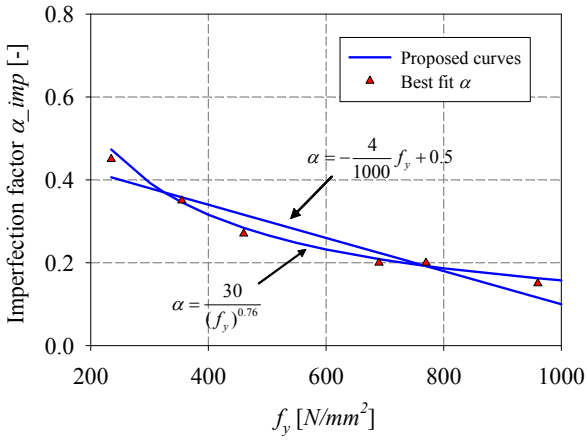

Figure 11: Variation of α factors based on the yield stress f_y for cold-formed sections, tested under compression

According to Figure 11, a relationship between the α factors and the yield stresses f_y can be established by using one of the following equations:

$$\alpha = -\frac{4}{1000} f_y + 0.5 \text{ for } f_y \geq 235 N/mm^2 \text{ (linear)} \quad (5)$$

Or alternatively (more accurate)

$$\alpha = \frac{30}{f_y^{0.76}} \text{ for } f_y \geq 235 N/mm^2 \text{ (non-linear)} \quad (6)$$

Table 1 summarizes the adopted parameters for the design curves of hot-rolled and cold-formed members of different steel grades subjected to pure compression, for $\chi_{CS} \geq 0.6$ cases.

Table 1: Design curves for hot-rolled and cold–formed members subjected to pure compression

Cross-section	Fabrication process	λ_0	α					
			$f_y = 235$ (N/mm^2)	$f_y = 355$ (N/mm^2)	$f_y = 460$ (N/mm^2)	$f_y = 690$ (N/mm^2)	$f_y = 770$ (N/mm^2)	$f_y = 960$ (N/mm^2)
RHS and SHS	Hot-rolled	0.2	0.21	0.21	0.21	0.13	0.13	0.13
	Cold-formed	0.2	0.45	0.35	0.27	0.20	0.20	0.15

4. High strength steel columns with highly slender sections

4.1. Influence of cross-section slenderness on the column's response

Figure 12 presents numerical results obtained by using shell models relative to class 3 (compact) and class 4 (slender) sections from different steel grades. Results for very slender sections ($\chi_{CS} < 0.6$) are included in this section and only the European (catalogue) cross-sections are considered. One may notice that the O.I.C. resistance curves begin to "decrease" when slender sections of high and ultra-high yield strength are used. For cold-formed sections, numerical results corresponding to very high steel grades tend to the curve defined for $f_y = 235\ N/mm^2$ ($\lambda_0 = 0.2$ and $\alpha = 0.45$). For the case of hot-rolled sections, numerical results corresponding to very high strength steel sections tend to a curve ($\lambda_0 = 0.2$ and $\alpha = 0.45$) lower than the one defined for $f_y = 235\ N/mm^2$ ($\lambda_0 = 0.2$ and $\alpha = 0.21$). When ultra-high strength steel is used, the handling of local buckling becomes crucial since the profiles made of such steel grades fall into the (very) slender range. It should be noted that the drop of resistance was noticed only for very slender sections of high steel grades when the European sections are contemplated, since the latter covers only a limited range of cross-section dimensions.

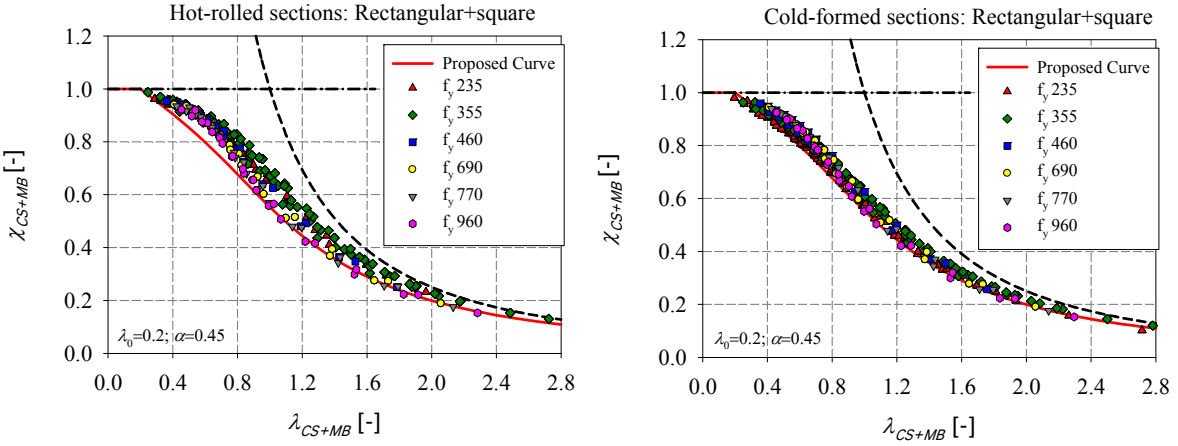

Figure 12: Numerical results of very slender SHS and RHS members of different steel grades under compression– a) hot-rolled – b) cold-formed

Figure 13 illustrates the deformed shape/yield pattern at failure of a slender section RHS 450x250x8 of high steel grade $f_y = 690\ N/mm^2$. Multiple buckling modes interact and give rise to a localization of the buckling patterns and yield extent. Peak loads are usually reached at the middle length of the member, when the section is loaded under compression. The stresses then decrease along the member length. Thus, a part of the member – less loaded under compression – is considered to be fully effective and provides a certain level of restraint to the section where failure finally happens.

When considering the O.I.C. approach (see equations (7) and (8)), or the Eurocode 3 procedure, the global interaction curves are computed by accounting for the most loaded cross-section local instabilities (see red circles in the equations below), located at mid-length (for the case of pure compression), from the overall behavior. This procedure does not lead to realistic load carrying capacities for very slender sections, where the resistance is greatly affected by the interaction between local and global buckling. Thus, considering the most loaded cross-section from the real behavior of the beam leads to inaccurate results, because only the most-loaded portion of the beam becomes ineffective.

$$\lambda_{CS+MB} = \sqrt{\frac{\chi_{CS}.R_{RESIST}}{R_{STAB}}} \tag{7}$$

$$\chi_{CS+MB} = \frac{R_{SHELL}}{\chi_{CS}.R_{RESIST}} \tag{8}$$

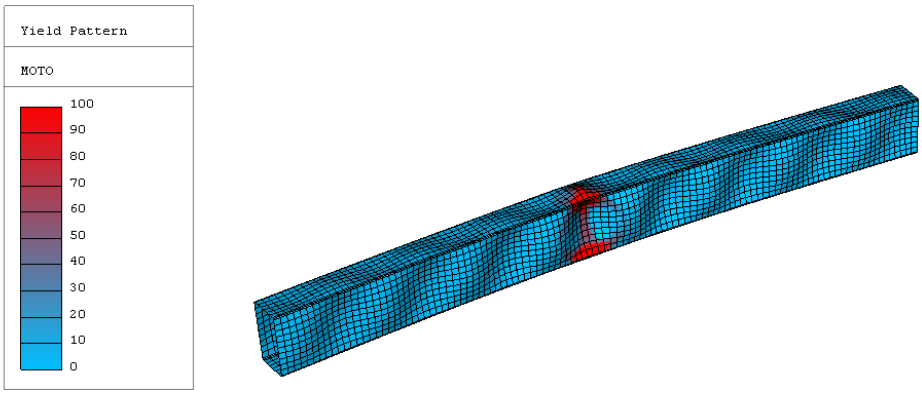

Figure 13: Deformed shape / yield pattern at failure of RHS_450x250x8 of steel grade $f_y = 690\ N/mm^2$ obtained through shell models

4.2. Second- order verification of mid-span cross-sections

A study was undertaken to rule the local-global interaction by considering a second-order cross-sectional check of the most heavily loaded section on the member (located at mid-span). Second-order effects were quantified by considering the following equation:

$$M^{II} = N_{Ed} v_{\max} \tag{9}$$

where v_{max} represents the maximum deflection reached at peak load (see Figure 14) and was obtained numerically with the use of FINELg shell models.

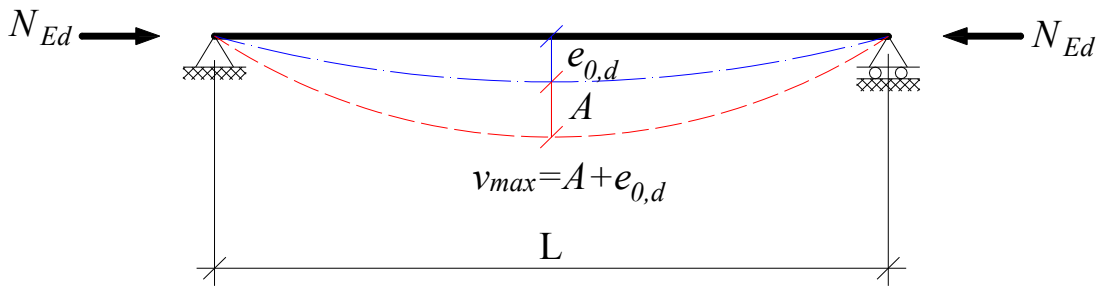

Figure 14: Simply supported member with initial imperfection

An initial equivalent deflection at mid-span $e_{0,d}$ was then back-calculated from numerical values of v_{max} from the following equation:

$$e_{0,d} = v_{\max}(1 - N_{Ed} / N_{cr}) \tag{10}$$

where N_{cr} is the flexural buckling critical load. $e_{0,d}$ shall be seen as the initial equivalent (generalized) imperfection that leads to an Equations (9)-(10)-based same $v_{\max}$ value as the one reached numerically. Results corresponding to hot-rolled and cold-formed sections are illustrated in Figure 15 and Figure 16 respectively, for class 1 and class 4 sections.

$$e_{0,d} = \frac{\eta}{W_{el}} A \tag{11}$$

where W_{el} is the elastic modulus and A is the gross cross-section area.

$$\eta = \alpha(\lambda - 0.2) \tag{12}$$

It is very classical in Ayrton-Perry approaches to adopt expressions for $e_{0,d}$ such as the ones of Equations (11) and (12), where η represents the generalized initial imperfection that can be used to estimate the effects of initial imperfections such as residual stresses, initial out of straightness or eccentrically applied forces on the buckling phenomenon. Because some of these initial imperfections are associated with the length of the member, different value of $e_{0,d}$ were obtained accordingly (see Figure 15 and Figure 16) depending on the member length (λ_{MB}).

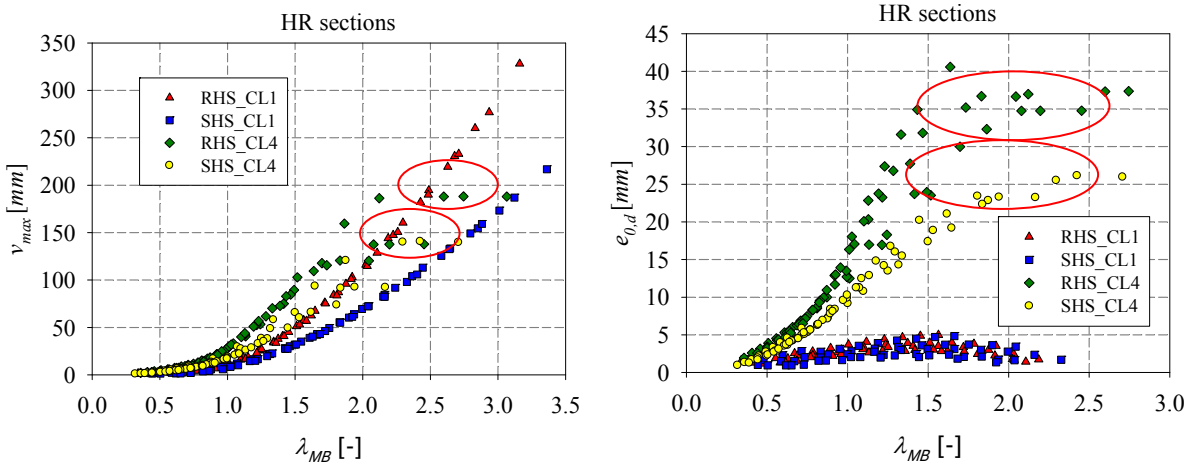

Figure 15: Maximum and back-calculated initial deflections reached at mid-span for hot-rolled sections

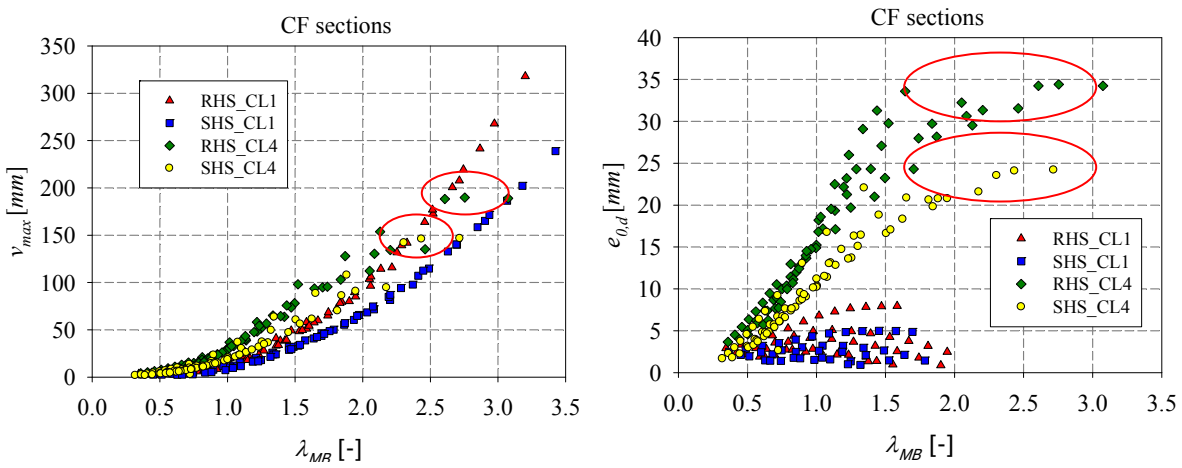

Figure 16: Maximum and back-calculated initial deflexions reached at mid-span for cold-formed sections

Clear tendencies are observed in the figures depending on the cross-sectional shape. It should be noted that, "lost points" on scatter (illustrated with the red circles) mark the influence a stronger local-global interaction. As illustrated, several corrections should be performed to remove the influence of the cross-section shape.

A verification of the most heavily cross-section was then performed, as acted by compression N_{Ed} and M^{II} from Equation (9) – the local-global interaction is taken into account through the inclusion of the second-order bending moment. Figure 17 compares $R_{REAL,\,MB,\,BEAM}$ and $R_{REAL,\,MB,\,SHELL}$ (representing the ultimate load multiplier of the column tested under pure compression, computed using shell and beam models, respectively, so as to witness global buckling modes only) to $R_{REAL,CS}$ (representing the ultimate load multiplier of the most heavily cross-section tested under $N+M^{II}$, computed using shell models).

The following conclusions can be drawn from these figures:

- Negligible differences are obtained by using either beam ($R_{REAL,\,MB,\,BEAM}$) and shell models ($R_{REAL,\,MB,\,SHELL}$) to compute the member resistance of stocky sections; although beam model gives always slightly higher results. This was obviously expected since cross-section instabilities are not likely to occur for compact sections;
- Beam models reach higher resistance (i.e. all the sections reach their plastic resistance) than shell ones (i.e. different values of resistance are reached: plastic or effective depending on the cross-section classification), slender sections exhibiting an important influence of local buckling have significantly lower resistance when modelled in shell elements than in beam elements. The difference reaches a value of 35% which cannot be ignored in design;
- Acceptable differences are obtained by comparing $R_{REAL,\,MB,\,SHELL}$ and $R_{REAL,\,CS,\,SHELL}$ for low values of relative slenderness λ_{CS+MB}. Member verification is showing safe results compared to the cross-section verification. A bigger disparity is seen with the increase of λ_{CS+MB};
- For low values of relative slenderness, it is clearly seen that significant difference arises when comparing $R_{REAL,\,MB,\,BEAM}$ to $R_{REAL,\,CS,\,SHELL}$. Beam models only able to witness global buckling regardless of the local buckling that may occur, are showing unsafe results for low values of relative slenderness. Indeed, the effect of local buckling is

mainly highlighted for low values of relative slenderness where the failure of the element is due to a lack of resistance and to cross-section buckling and not because of member instability. For high values of relative slenderness, global buckling becomes determinant, thus closer tendencies are observed by comparing $R_{REAL,\ MB,\ BEAM}$ to $R_{REAL,\ CS,\ SHELL}$.

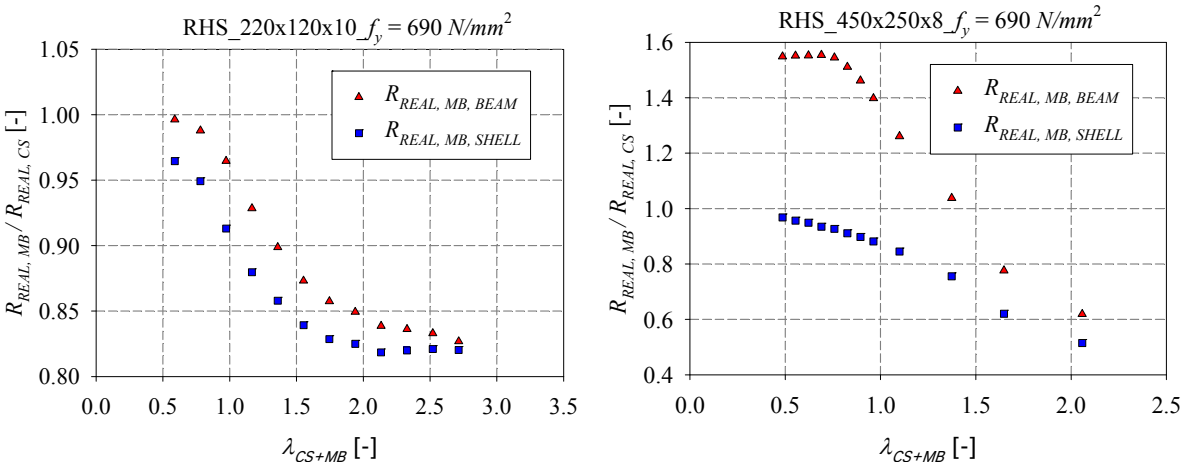

Figure 17: $R_{REAL,\ MB}$ / $R_{REAL,\ CS}$ graphical representation as a function of λ_{CS+MB}

4.3. Exaggeratedly slender cross-sections

An additional set of invented sections was analyzed, in an attempt to examine the O.I.C. approach under more severe circumstances, i.e. when the interaction between local and global instabilities becomes crucial and deserves special attention. Invented sections, having highly slender components are used in order to better visualize more distributed results along higher slenderness, since the European sections covers only a limited range of cross-section slenderness. Figure 18 illustrates the adopted invented cross-sectional dimensions.

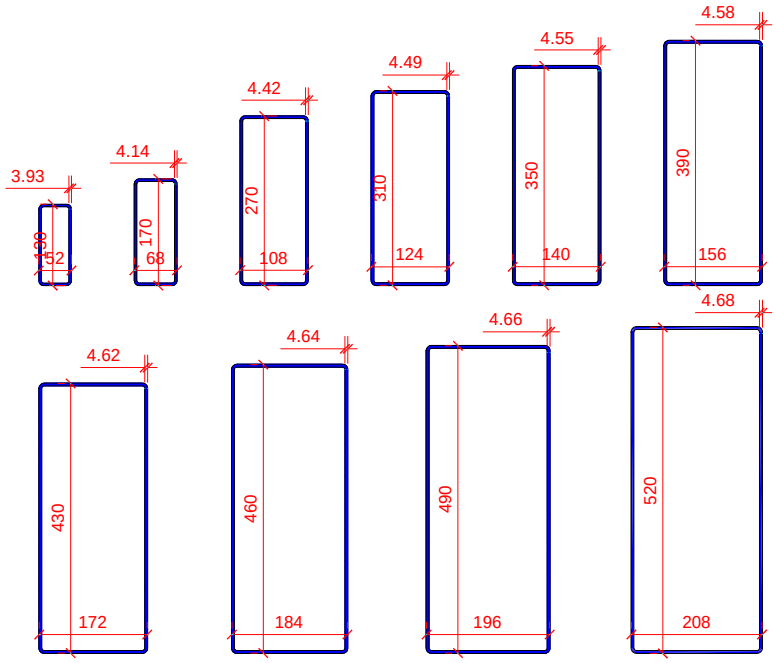

Figure 18: Invented cross-section dimensions

As illustrated in Figure 19, "anomalies" (i.e. different behaviors) appear as the O.I.C. resistance curves begin to decrease when slender sections of high and ultra-high yield strength are used. For sake of clarity, only results of hot-rolled sections of nominal steel grades $f_y = 690\ N/mm^2$, $f_y = 770\ N/mm^2$ *and* $f_y = 960\ N/mm^2$ are given here.

Local instability is greater with an increase in cross-section slenderness λ_{CS}; the sections exhibit an important influence of local buckling on the overall response of the member in this case. Lower curves should be derived for this type of sections. Appropriate curves are derived by using the Ayrton-Perry approach and the imperfection factors α were locally determined through a best-fit procedure: different values of α were selected depending on the corresponding cross-section slenderness. The local-global interaction is thus taken into account by means of appropriate α factors. The adopted values of α (obtained through best-fit calculations) are represented with blue square dots in Figure 20. A comparison of the proposed calibrated expression of α to the analytical one has been done. Analytical values of α were calculated according to Equation (13), where η was derived according to Equation (14), and are represented with green triangular dots in Figure 20.

$$\eta = \alpha(\lambda - 0.2) \tag{13}$$

$$(1-\chi)(1-\chi\lambda^2) = \eta\chi \tag{14}$$

The different analytical values of α obtained for an identical cross-sectional slenderness λ_{CS} correspond to different member lengths: according to Equation (13), η represents the generalized initial imperfection that can be used to estimate the effects on the buckling phenomenon of initial imperfections such as residual stresses, initial out of straightness or eccentrically-applied forces. Because some of these initial imperfections are linked with the length of the member, different value of α were accordingly obtained depending on the member length.

It is to be noted that the imperfection factor α also accounts for the cross-section shape and that it was derived so as to provide safe-sided approximations. The red lines in Figure 20 show the relation that is then proposed between α and λ_{CS}. It can be clearly seen that the proposed equations are describing well enough the beam-column resistance. For low values of relative slenderness ($\lambda_{CS} < 0.8$), where global buckling is dominant, constant values of α are proposed. For higher values of relative slenderness ($0.8 < \lambda_{CS} < 2.0$), local buckling becomes more relevant: the O.I.C. resistance curves decrease and the values of the imperfection factor α increase with the increase of λ_{CS}. Finally, for high values of relative slenderness ($\lambda_{CS} > 2.0$), the standard O.I.C. buckling curves become more "stable" (i.e. suitable without any modification aimed at accounting for the local/global coupling) after a progressive drop starting from $\lambda_{CS} > 0.8$ and therefore a constant value of α is proposed again.

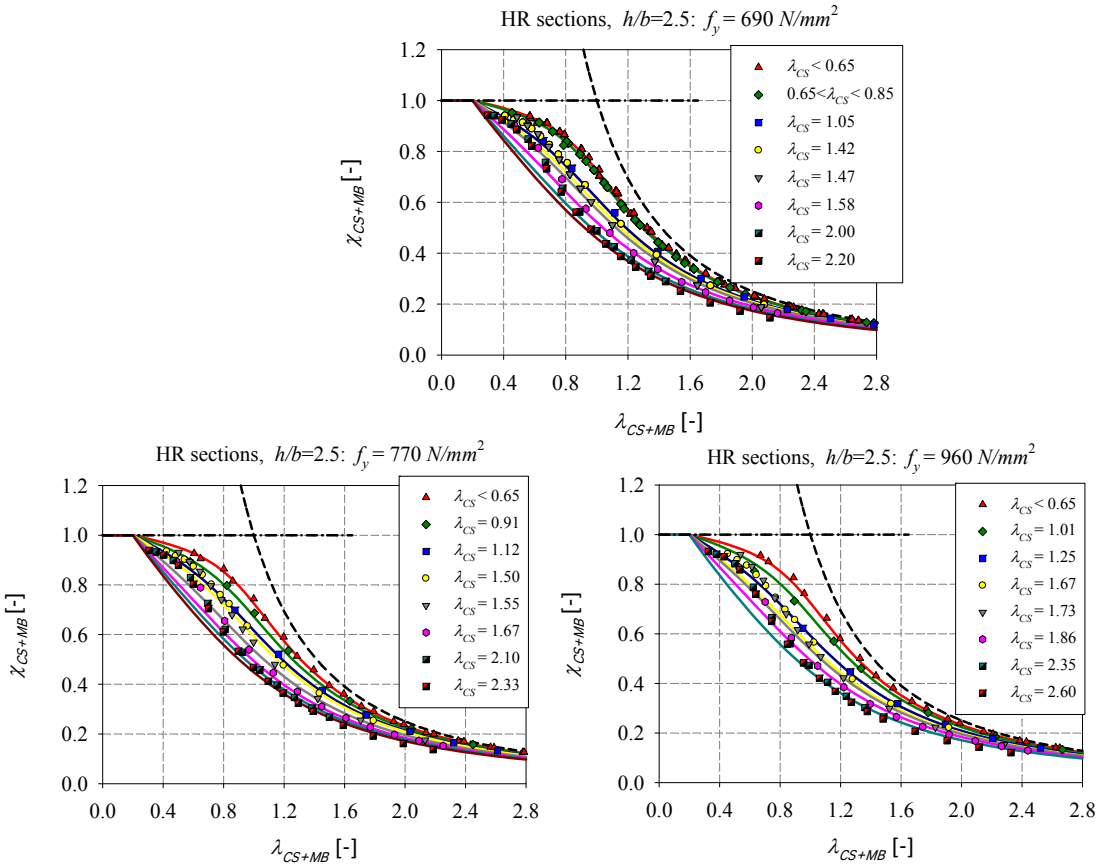

Figure 19: Numerical member results for hot-rolled "exaggerated" slender sections under compression

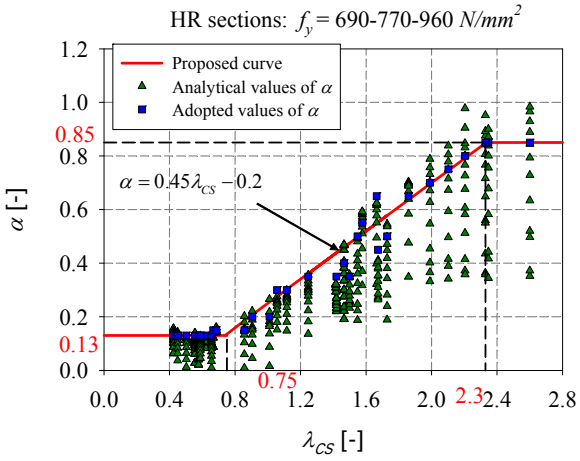

Figure 20: Comparison of analytical factors α with the adopted ones (obtained through the best-fit procedure) of hot-rolled sections in compression

Alternatively, a complementary parameter β could be added to the Ayrton-Perry format in order to reduce the differences between the proposed curves and the F.E. results in the slenderness range $0.4 \le \lambda_{CS+MB} \le 0.8$. Such a factor β was added to the proposed curves following Equations (15) and (16).

$$\chi_{CS+MB} = \frac{1}{\phi_{CS+MB} + \sqrt{\phi_{CS+MB}^{\ 2} - \beta\lambda_{CS+MB}^{\ 2}}} \le 1 \tag{15}$$

$$\text{where } \phi_{CS+MB} = 0.5\left(1 + \alpha\left(\beta\lambda_{CS+MB} - \lambda_0\right) + \lambda_{CS+MB}^{\ 2}\right) \tag{16}$$

Figure 21a illustrates the results obtained through such curves, for hot-rolled sections of yield stress $f_y = 235\ N/mm^2$, where the imperfection factor α and the β factor were locally determined through a best-fit procedure. Different values of α and β factors were chosen depending on the corresponding cross-section slenderness. The adopted values are represented in Figure 21b. A relation was then derived between the proposed α (represented by the blue dots on the figure), β (represented by the green dots) and λ_{CS}.

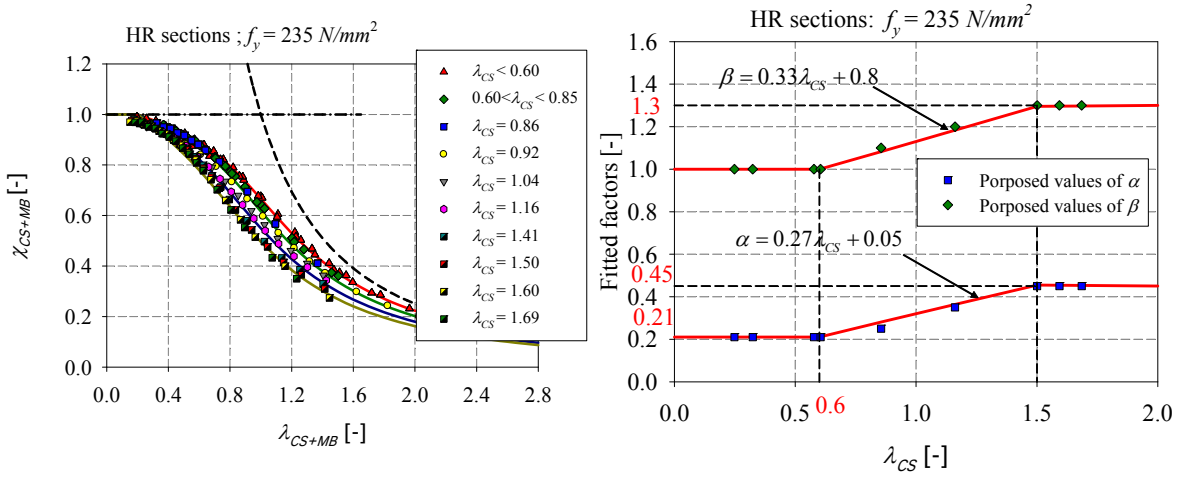

Figure 21: Numerical results for hot-rolled members with "exaggeratedly" slender sections of steel grade $f_y = 235\ N/mm^2$ tested under compression – a) proposed O.I.C. curves – b) fitted factors

4.4. Local/global interaction factor

Another way of handling the local buckling of slender sections of high steel grades is the determination of a local/global interaction factor such as detailed in the present paragraph. The figures presented hereafter show results of hot-rolled and cold-formed sections made of different steel grades and tested under pure compression. In Figure 22, only the European (catalogue) cross-sections are considered; however, in Figure 23, members having a yield stress of $f_y = 690\ N/mm^2$ include both the European an the invented cross-sections.

The results obtained by means of shell F.E. models where both local and global instabilities are accounted for show that the influence of the section sensitivity to local buckling is important. For both types of sections (the European and the invented ones), one may notice that the O.I.C. resistance curves safely represent the actual resistance of the members even for high strength steel sections, except when $\chi_{CS} < 0.6$ (i.e. high influence of local buckling instabilities). The O.I.C. curves begin to decrease when slender sections of high yield strength are used.

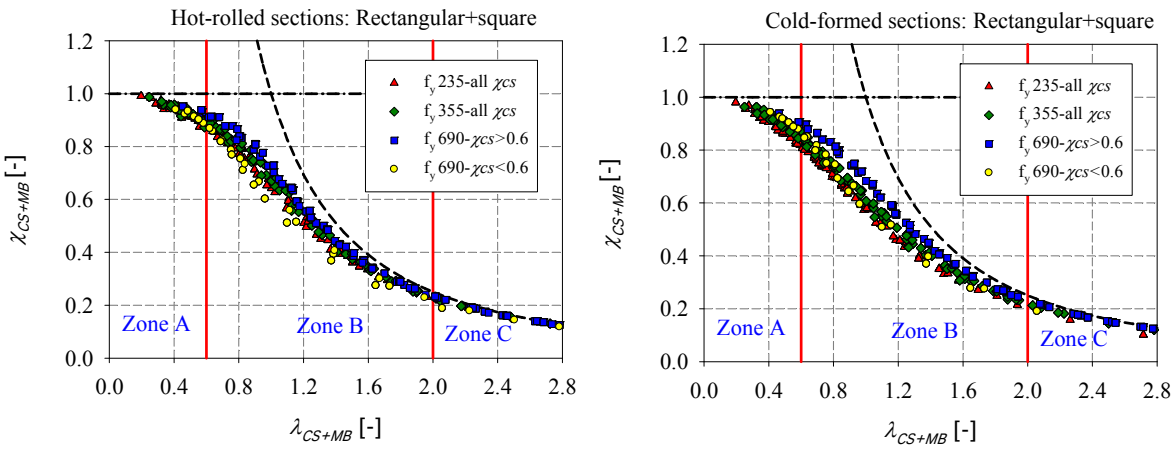

Figure 22: Numerical member results for "European catalogue"– a) hot-rolled sections – b) cold-formed sections

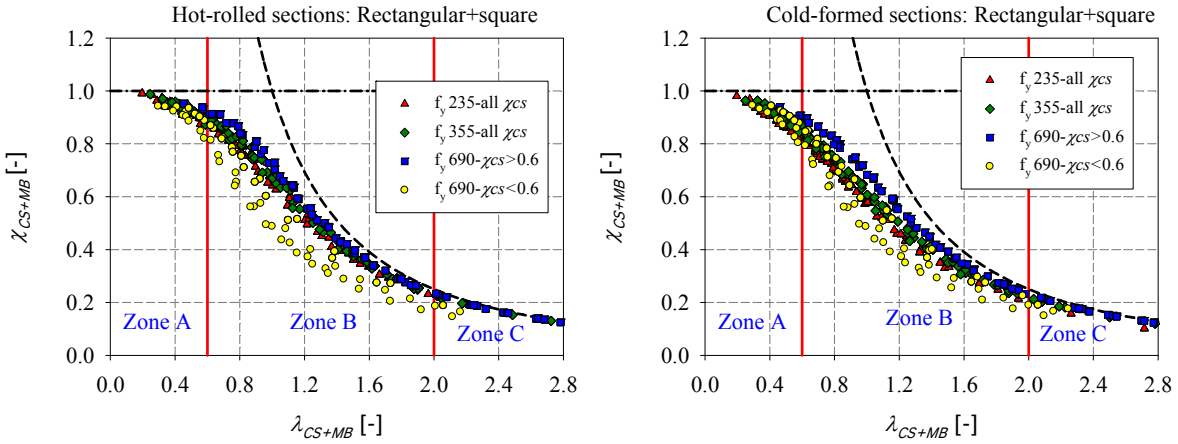

Figure 23: Numerical member results including "exaggerated" a) hot-rolled sections – b) cold-formed sections

In order to better visualize the influence of the cross-section behavior on the overall response when the coupling is high, Figure 24 illustrates the load-displacement curve of an RHS 450x250x8 of nominal steel grade $f_y = 690\ N/mm^2$ tested under pure compression. For illustrative purposes, the geometry, loading, column length and steel grade have been chosen so as local buckling to be predominant and global (flexural) buckling to be limited.

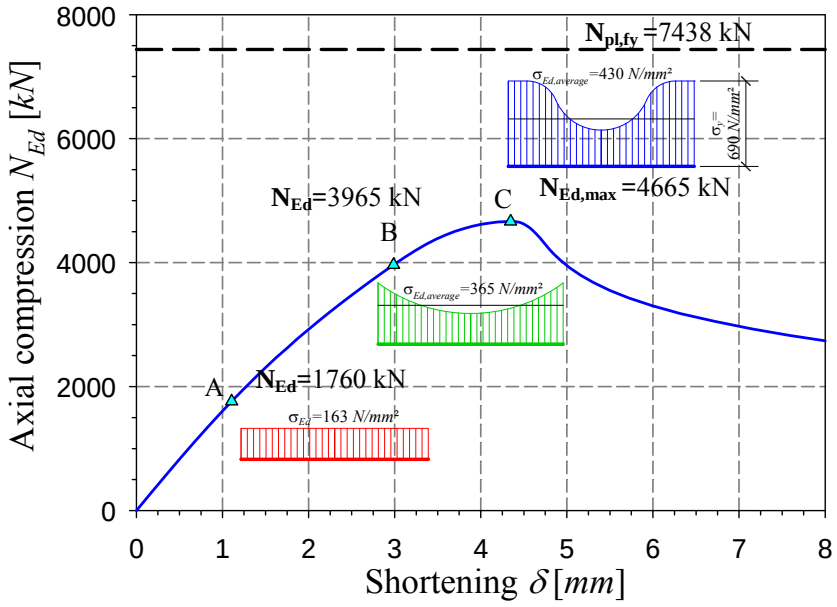

Figure 24: Numerical load-displacement results – RHS HR 450x250x8

Several stages A, B and C can be separated; at first (stage A), the stresses along an element of the section (flat face) increase uniformly with the applied load. At this point, the compression stress σ_{Ed} is distributed uniformly and elastically across the plates of the section, as shown for point A for example where the applied load and stress are equal to $N_{Ed} = 1760\ kN$ and $\sigma_{Ed} = 163\ N/mm^2$, respectively.

After local buckling develops, the uniform stress distribution tends to a non-uniform pattern as shown for point B for example, where the applied load and average stress are equal to $N_{Ed} = 3965\ kN$ and $\sigma_{Ed,average} = 365\ N/mm^2$.

This non-uniform distribution is accentuated with an increase in loading leading to greater and gradually stresses redistributions until reaching the ultimate load as shown for point C where the applied load and average stress are equal to $N_{Ed} = 4665\ kN$ and $\sigma_{Ed,average} = 430\ N/mm^2$, respectively. At peak load, local buckling is very pronounced, and the distribution of stresses becomes highly non-linear – only the fibers at edges can reach the yield stress $f_y = 690\ N/mm^2$.

As noticed in Figure 22 and in Figure 23, members' real resistance show analogous load-carrying behavior in the three different ranges of column slenderness, summarized as follow:

- At very low slenderness (in Figure 25, $\lambda_{CS+MB} < 0.6$: zone A), the cross-sectional resistance dominates and the effect of local buckling on the overall member's response is strong. The failure of the element is mostly due to cross-section buckling and not to member instability. The average stress level *in the member* in this case is close to the average level of stresses at peak load for point C (see cross-section studies, Figure 24). The O.I.C. approach can accurately treat this local/global buckling interaction for highly slender cross-sections at zone A, since the definition and use of a local/global slenderness λ_{CS+MB} can safely represent the member real resistance which is further obtained by using the equation below:

$$R_{REAL} = \chi_{CS+MB} \cdot \chi_{CS} \cdot R_{RESIST} \tag{17}$$

where $\chi_{CS+MB} \approx 1.0$

- With increasing slenderness ($0.6 < \lambda_{CS+MB} < 2$: zone B), members fail because of both local (i.e. cross-section instabilities) and global (i.e. member instabilities) buckling modes (i.e. pronounced coupled instabilities); although the cross-section may be very slender, local buckling is less pronounced in this case. Slender sections exhibiting an important influence of local buckling have a lower resistance and the O.I.C. resistance curves begin to decrease in this case. At member's peak load, the average level of stresses in members is much lower than for zone A – due to the global flexural buckling that limits the stresses at peak – and is closer to the stress distribution of point B (see cross-section studies, Figure 24). The member real resistance shall be calculated in this case by considering a higher value for χ_{CS} and such that this value does not exceed 1.0;
- In the high slenderness range ($\lambda_{CS+MB} > 2.0$: zone C), member buckling is dominated by elastic behavior. Elastic global buckling is predominant and local buckling shall not develop significantly. The average level of stresses in members reached at peak load is small and is close to the constant elastic distribution of stress for point A (see cross-section studies, Figure 24). The cross-section shall be considered as fully effective since local buckling tends to be very limited. The member real resistance must be calculated in this case by considering $\chi_{CS} = 1.0$.

Accordingly, and in order to determine accurately the interaction between local and global instabilities for the case of high strength steel sections of highly slender components, a local/global interaction factor $f_{coupling\ L/G}$ can be added to Equation (3) and Equation (4). The penalty factor χ_{CS+MB} and the relative slenderness λ_{CS+MB} according to the O.I.C. approach become:

$$\lambda_{CS+MB} = \sqrt{\frac{\chi_{CS} \cdot f_{coupling\ L/G} \cdot R_{RESIST}}{R_{STAB,MB}}} \tag{18}$$

$$\chi_{CS+MB} = \frac{R_{REAL}}{\chi_{CS} \cdot f_{coupling\ L/G} \cdot R_{RESIST}} \tag{19}$$

where $f_{coupling\ L/G}$ is such that (see Figure 25):

- At very low slenderness (zone A): $\chi_{CS} \cdot f_{coupling\ L/G} = \chi_{CS} \Rightarrow f_{coupling\ L/G} = 1$;
- With increasing slenderness (zone B): $\begin{matrix} \chi_{CS} \cdot f_{coupling\ L/G} \le 1 \\ \chi_{CS} \cdot f_{coupling\ L/G} \ge \chi_{CS} \end{matrix} \Rightarrow f_{coupling\ L/G} \le 1/\chi_{CS}$;
- In the high slenderness range (zone C): $\chi_{CS} \cdot f_{coupling\ L/G} = 1 \Rightarrow f_{coupling\ L/G} = 1/\chi_{CS}$.

Additional investigations are currently under development to determine safe-sided equations to represent $f_{coupling\ L/G}$.

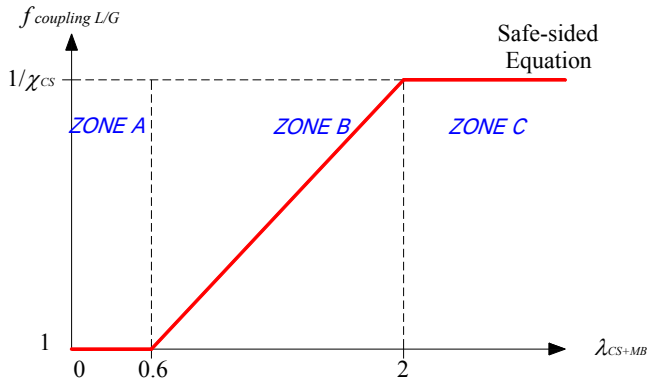

Figure 25: Safe-sided equation for $f_{coupling\ L/G}$ values

5. Conclusions and future steps

The peculiarities of high-strength materials (σ-ε curves) and sections (different production routes and imperfections levels) are only superficially studied and addressed in design codes. Generally, the treatment of local/global instabilities in the Eurocode and other international design codes is seen as too cumbersome by many designers and does not take full advantage of already-available numerical computational methods.

EN 1993 covers steel grades up to $f_y = 460\ N/mm^2$, and with small adjustments, up to $f_y = 690\ N/mm^2$. The existing design rules and requirements are examined in this paper with regard to more economic and feasible design rules, covering steel grades up to $f_y = 960\ N/mm^2$.

New design proposals providing increased resistance capacities – for the particular case of cold-formed sections – and removing the unnecessary steps in the existing design provisions are proposed based on the O.I.C. concept. The O.I.C. aims at developing new, direct design rules regarding strength and stability checks. Addressing both usual steel grades as well as tomorrow's high strength steels, this approach allows for more economic, innovative, "thin-walled" hollow section members.

The particular case of very slender members (exaggeratedly slender cross-sections) demonstrated some kind of specific response, not so obvious to treat in traditional ways. Special care was taken in designing these members that represent a special group of elements, through two different procedures: curve-fitting of so-called α-values and use of local/global interaction factors.

For now, the behavior and design of compact to slender high strength steel beam-column members were investigated for RHS and SHS cross-sections subjected to simple load cases. Other contributions are under way to investigate the behavior of high strength steel members under combined loading situations that provide similar responses as the pure compression load cases.

Acknowledgements

CIDECT, by means of financial and technical support within research project "HOLLOPOC", is gratefully acknowledged.

References

Ayrton W.E. & Perry J. (1886). "On Struts."*The engineer,* Vol.62.

Boissonnade N. & Somja H. (2012). "Influence of Imperfections in FEM Modelling of Lateral Torsional Buckling." *Proceedings of the Annual Stability Conference, Structural Stability Research Council,* Grapevine, Texas, April 18-21.

ECCS publications (1987). "Ultimate Limit State Calculation of Sway Frames with Rigid Joints".

Epiney V. (2015). "Resistance et Stabilité Des Éléments En Acier Fléchis et Tendus." *Master HES-SO,* Ingénierie du Territoire MIT.

CEN (Comité Européen de Normalisation. (2005). "Eurocode 3: Design of Steel Structures, Part 1–1: General rules and rules for buildings (EN 1993-1-1)", Brussels.

CEN (Comité Européen de Normalisation) (2007). "Eurocode 3: Design of Steel Structures, Part 1–12: Additional Rules for the Extension of EN1993 up to Steel Grades S700"

Greish & ULg (1999). "FINELg, Non Linear Finite Element Analysis Software." *University of Liege - The engineering office Greisch*

Hayeck M. (2016). "Development of a New Design Method for Steel Hollow Section Members Resistance." University of Liege, Belgium.

Key P.W. (1988). "The Behavior of Cold-Formed Square Hollow Section Columns." University of Sydney, Australia.

Nseir J. (2015). "Development of a New Design Method for the Cross-Section Capacity of Steel Hollow Sections." University of Liege, Belgium.

Nseir J, Hayeck M., Saloumi E., Boissonnade N. (2016). "Influence of imperfections on the local buckling response of hollow structural shapes". *Proceedings of the Annual Stability Conference, Structural Stability Research Council*, Orlando, Florida, April 12-15.

Rasmussen K.J.R. (2003). "Full-Range Stress-Strain Curves for Stainless Steel Alloys." *Journal of Constructional Steel Research*, 59, 47-61.

Semi-Comp (2007). "Plastic member capacity of semi-compact steel sections – a more economic design (Semi-Comp)". 2007. *Final report (01/01/06 – 30/06/07)* – RFCS – Steel RTD (Contract RFS-CR-04044).